J. Fluid Mech. (2002), *vol.* 457, *pp.* 295–324.
DOI: 10.1017/S0022112001007662 Printed in the United Kingdom

Gravity currents in rotating channels. Part 1. Steady-state theory

By J. N. HACKER[1]† AND P. F. LINDEN[2]

[1]Department of Applied Mathematics and Theoretical Physics, University of Cambridge, Silver Street, Cambridge CB3 9EW, UK

[2]Department of Applied Mechanics and Engineering Science, University of California, San Diego, 9500 Gillman Drive, La Jolla, CA 92093-0411, USA

(Received 27 October 1998 and in revised form 24 October 2001)

A theory is developed for the speed and structure of steady-state non-dissipative gravity currents in rotating channels. The theory is an extension of that of Benjamin (1968) for non-rotating gravity currents, and in a similar way makes use of the steady-state and perfect-fluid (incompressible, inviscid and immiscible) approximations, and supposes the existence of a hydrostatic 'control point' in the current some distance away from the nose. The model allows for fully non-hydrostatic and ageostrophic motion in a control volume V ahead of the control point, with the solution being determined by the requirements, consistent with the perfect-fluid approximation, of energy and momentum conservation in V, as expressed by Bernoulli's theorem and a generalized flow-force balance. The governing parameter in the problem, which expresses the strength of the background rotation, is the ratio $W = B/R$, where B is the channel width and $R = (g'H)^{1/2}/f$ is the internal Rossby radius of deformation based on the total depth of the ambient fluid H. Analytic solutions are determined for the particular case of zero front-relative flow within the gravity current. For each value of W there is a unique non-dissipative two-layer solution, and a non-dissipative one-layer solution which is specified by the value of the wall-depth h_0. In the two-layer case, the non-dimensional propagation speed $c = c_f(g'H)^{-1/2}$ increases smoothly from the non-rotating value of 0.5 as W increases, asymptoting to unity for $W \to \infty$. The gravity current separates from the left-hand wall of the channel at $W = 0.67$ and thereafter has decreasing width. The depth of the current at the right-hand wall, h_0, increases, reaching the full depth at $W = 1.90$, after which point the interface outcrops on both the upper and lower boundaries, with the distance over which the interface slopes being $0.881R$. In the one-layer case, the wall-depth based propagation speed Froude number $c_0 = c_f(g'h_0)^{-1/2} = 2^{1/2}$, as in the non-rotating one-layer case. The current separates from the left-hand wall of the channel at $W_0 \equiv B/R_0 = 2^{-1/2}$, and thereafter has width $2^{-1/2}R_0$, where $R_0 = (g'h_0)^{1/2}/f$ is the wall-depth based deformation radius.

1. Introduction

A gravity current is a flow of fluid of one density into a fluid of different density along a predominantly horizontal boundary or density interface (Simpson 1997). The flow results from the hydrostatic pressure contrast imposed by the density difference, the depth of the gravity current and the horizontal boundary. Gravity currents occur

† Present affiliation: Arup Research and Development, 13 Fitzroy Street, London W1T 4BQ, UK.

in a wide range of situations in the environment, particularly where transient events generate horizontal density gradients that subsequently steepen to form sharp fronts (Simpson & Linden 1989). An important feature of the flow is the unstable and turbulent nature of the leading edge of the current, which typically produces mixing between the gravity current and ambient fluid surroundings (Hacker, Linden & Dalziel 1996). These mixing processes, together with the capacity of the flow to transport fluid over large distances, make gravity currents important in many environmental and industrial situations, particularly where the transport and distribution of passive or active scalars is of concern.

Smaller-scale environmental gravity currents are often relatively unaffected by the effects of the Earth's rotation (Simpson 1997), but on larger scales these effects can have a profound influence on the dynamics (Griffiths 1986). The most well-studied paradigm is a gravity current propagating in a rectangular channel. In the absence of background rotation, the gravity current extends across the complete width of the channel and has essentially a two-dimensional structure. When background rotation is present, the gravity current experiences a Coriolis force, which, for northern-hemisphere sense of rotation (henceforth assumed, with apologies to southern hemisphere readers) acts into the right-hand wall of the channel. (By convention the term 'right-hand' is used with reference to an observer facing in the direction of propagation; the term 'left-hand' will be used similarly.) Over a timescale of the order of f^{-1}, where f is the Coriolis frequency, this Coriolis force brings the along-channel flow into geostrophic balance by establishing an across-channel depth gradient. At the leading edge of the current, on the other hand, the kinematic requirement of zero flow across the right-hand boundary removes the component of Coriolis force parallel to the boundary, so that the dynamic balance at the nose is essentially an ageostrophic one, between inertia and pressure, similar to that in the non-rotating case. This combination of geostrophic and ageostrophic dynamics is essentially that supporting Kelvin wave propagation, and rotating gravity current fronts are sometimes considered to be shock-wave forms of long internal Kelvin waves.

Since the current is buoyancy-driven, the front speed $c_f \sim (g'h_0)^{1/2}$, where g' is the reduced gravity based on the density difference between the gravity current and ambient fluids and h_0 is the depth of the gravity current at the right-hand wall. Scaling then indicates that in the geostrophic region away from the nose, the across-channel depth gradient is of order h_0/R_0 where $R_0 = (g'h_0)^{1/2}/f$ is the Rossby radius of deformation. The non-dimensional parameter

$$W_0 \equiv \frac{B}{R_0} = \frac{fB}{(g'h_0)^{1/2}}, \tag{1.1}$$

where B is the width of the channel, therefore gives a measure of the across-channel depth variation relative to the wall-depth h_0, or, if the current does not extend across the complete width of the channel, gives a measure of the width of the channel relative to the width of the current. This parameter, therefore, reflects the strength of the background rotation in a particular situation. (The parameter W_0 may also be viewed as the square root of a rotating Froude number or as an inverse Rossby number based on the velocity scale $(g'h_0)^{1/2}$ and lengthscale B.) For the two-layer case, which will be considered later, it is often more convenient to base W_0 on the total ambient fluid depth H, and so we also define

$$W \equiv \frac{B}{R} = \frac{fB}{(g'H)^{1/2}}, \tag{1.2}$$

in which $R = (g'H)^{1/2}/f$ is the deformation radius based on the total depth H.

1.1. *Rotating gravity currents in the environment*

Gravity current fronts with finite values of W_0 occur in a wide variety of situations in the environment. Oceanic examples include: flows in broad estuaries (O'Donnell 1993); coastal gravity currents such as the Kyucho (Takeoka, Akiyama & Kikuchi 1993, and references contained therein); tidally modulated exchange flows between coastal- and semi-enclosed seas (e.g. Hickey *et al.* 1991; LeBlond *et al.* 1991); and benthic flows in coastal and deep-ocean channels (e.g. Saunders 1994; Signori, Münchow & Haidvogel 1997; Lavín, Godínez & Alvarez 1998). In the atmosphere, large-scale gravity currents also occur propagating along major mountain ranges (e.g. Volkert, Weikman & Tafferner 1991, and references contained therein), and while usually only affected by one lateral boundary, may experience effectively finite values of W_0 if subject to lateral blocking effects due to the synoptic-scale flow. The same is also true of gravity currents in the oceans flowing predominantly along only one lateral boundary, such as a coastline, since these can be affected by blocking effects due to the potential vorticity gradients set up by the presence of strong topographic features, such as the shelf-break.

We note that the term 'gravity current' is also sometimes used to refer to buoyancy-driven flows that are entirely geostrophic, for example those produced by geostrophic adjustment. In this paper, however, we will be primarily concerned with flows of the type described above, in which the gravity current has an ageostrophic leading edge, since the presence of the ageostrophic front can place important restrictions on the structure and speed of the geostrophic part of the flow. In the above examples, fronts of this type are produced by the essentially transient nature of the situation. It is also possible, however, that such fronts occur in flows generally considered to be more persistent and steady. For example, along-shore propagating fronts have been observed in buoyancy-driven coastal currents such as the Alaskan Coastal Current (Royer 1981; Alhnäs, Royer & George 1987) and the Norwegian Coastal Current (Ikeda *et al.* 1989), and it is likely that such fronts occur in other flows of this type (Hacker 1996, 1998).

1.2. *Previous work*

Most work on rotating gravity current fronts of the type described above (Stern, Whitehead & Hua 1982; Griffiths & Hopfinger 1983; Kubokawa & Hanawa 1984) has focused on the one-layer strongly rotating case of $W_0 \gg 1$ and $h_0/H \ll 1$. Wang (1985) and Nof (1987), however, have considered the two-layer case, at moderate values of W_0.

Wang (1985) reported a numerical simulation of a full-depth lock-release gravity current in a rotating channel propagating along a no-slip surface for $W = 1.8$. The maximum width of the current was approximately half the width of the channel and the maximum depth was close to the total depth H. The non-dimensional propagation speed $c \equiv c_f/(g'H)^{1/2}$ remained steady at $c = 0.49$ for approximately 7 lock-lengths of propagation. This value was slightly greater than that of $c = 0.46$ obtained in a non-rotating control simulation.

Nof's (1987) study was theoretical and made use of an approach developed by Benjamin (1968) for the non-rotating case. This approach supposes the gravity current and ambient surroundings to be composed of two distinct perfect fluids (incompressible, inviscid and immiscible), that the flow relative to the nose and speed of propagation are steady, and that the flow is controlled from a hydrostatic region within the gravity current some distance from the nose where the interface asymptotes to the horizontal (henceforth the 'control-point'). The solution is then obtained by imposing

the conditions, consistent with the above approximations, of energy and momentum conservation in a control volume V connecting the flow at the control point to the ambient flow far ahead of the gravity current. Benjamin's calculation shows that there is only one two-layer non-dissipative flow. In this solution, the fractional depth of the gravity current at the control point $\eta_0 = \frac{1}{2}$ and the non-dimensional propagation speed $c = \frac{1}{2}$. Benjamin also made a free-boundary calculation to determine the shape of the interface in the energy-conserving flow. He went on to consider the possible effects of dissipation by including uniform loss of energy on ambient fluid streamlines, and showed that dissipative solutions are possible when $\eta_0 < \frac{1}{2}$. For these solutions, the propagation-speed Froude number $c_0 \equiv c_f/(g'h_0)^{1/2}$ increases from the non-dissipative value of $2^{-1/2}$ to the value of $2^{1/2}$ as η_0 decreases, with the flow becoming non-dissipative again in the one-layer limit $\eta_0 \to 0$.

Laboratory experiments carried out in a 'steady-state' apparatus (Britter & Simpson 1978; Simpson & Britter 1979) indicate that the variation of c_0 with fractional depth predicted by Benjamin's dissipative theory occurs, at least qualitatively, in turbulent, miscible, Boussinesq gravity currents. There appears to be less consensus in the literature as to how relevant the non-dissipative two-layer solution is to real flows. There is, however, a reasonable body of evidence from laboratory and numerical observations to suggest that gravity currents with characteristics close to the non-dissipative solution occur in a wide-range of situations† and therefore that this solution may be fundamental to the dynamics of non-rotating gravity currents.

In any case, a non-dissipative theory must be seen as a necessary first step to the development of a Benjamin-like theory for the rotating case. Nof (1987) considered this problem for the case of gravity currents with zero internal potential vorticity (PV) propagating in a rectangular rotating channel. He supposed the flow at the control point to be geostrophic, and the interface to outcrop at some position across the channel so that the current had finite width b^*. Under these assumptions, Nof found that non-dissipative two-layer solutions were possible for the range of rotation strengths $0.6 \lesssim W \lesssim 1.8$. The solution was unique for each value of W. The relative width $b = b^*/B$ decreased monotonically from unity to approximately 0.65 and the fractional depth of the current at the right-hand wall η_0 increased from approximately 0.67 to unity at the endpoint of the solution. The Froude number c_0 showed very little variation, increasing slowly with W from the value of 0.811 to a maximum of 0.824.

1.3. *Outline of the paper*

In this paper and two accompanying papers (Hacker & Linden 2002*a*, *b*, hereinafter referred to as Parts 2 and 3) we report a study which considers the dynamics of gravity currents in rectangular channels at levels of rotation W connecting the non-rotating and strongly rotating regimes. The first two papers are theoretical and reconsider the problem considered by Nof (1987) discussed above. There are several reasons for this. First, since Nof's solution begins at a finite value of W, it is not clear how this solution relates to Benjamin's non-rotating solution, and moreover, what types of solution exist in other parts of the W parameter space. Secondly, Nof's mathematical treatment has certain shortcomings. For example, the derivation given of the rotating flow-force balance relies on the hydrostatic assumption. Nof commented that some of the dynamical constraints are redundant but gave no reasons for this. Also, his

† These observations do not appear to have been considered collectively in the literature, and are discussed in Appendix A.

analysis relied heavily on the use of an alegebraic manipulation package, so that the physical significance of the equations was lost at an early stage. Here, it will be shown that Nof's conclusion that non-dissipative solutions are only valid for a restricted range of W is not correct, and arises from the assumptions made regarding the structure of the flow. By considering different types of flow structure, it will be possible to determine non-dissipative solutions for all values of W. A derivation of the rotating flow-force that does not rely on the hydrostatic assumption will also be given, and we discuss why some of the constraint equations become redundant. In these and other respects we believe our treatment to be substantially more rigorous and complete than that given by Nof (1987).

In this paper we formulate the problem for the case of zero-front relative flow within the gravity current, which is the simplest case mathematically and elucidates much of the important physics. In Part 2 this assumption will be relaxed, and solutions will be determined for the case of uniform PV within the gravity current, including the case of zero PV considered by Nof. Applying Benjamin's method in the non-rotating case is more difficult than in the non-rotating case – because the flow becomes essentially three-dimensional and there is also a need to conserve PV within the perfect fluid assumption – and in both papers we will consider only the non-dissipative case. In Part 3 we will report the results of laboratory experiments designed to assess the applicability of the steady-state theory to real situations. It will be shown that the theory gives good predictions for the propagation speed and structure of high-Reynolds-number gravity currents, of a type similar to those occurring in the environment.

The structure of this first paper is as follows. In § 2, the model and governing equations are formulated and then in § 3 these equations are solved for the two-layer case and the solutions discussed. In § 4 the one-layer case is considered in the context of the theory developed in § 2. Finally, in § 5, the results are summarized and the conclusions are given.

2. Formulation

The situation to be considered is shown in figure 1. A gravity current of density ρ_c flows into an ambient fluid of density ρ_a and depth H contained in a long horizontal rectangular channel of width B. The channel rotates about a vertical axis with uniform angular frequency Ω. The ambient fluid is quiescent far ahead of the nose, and both fluids are inviscid, incompressible, and immiscible. We suppose that $|\Delta\rho|/\rho_a = |\rho_a - \rho_c|/\rho_a \ll 1$ and $\rho_a \gg \rho_u$, the density of any overlying layer, and correspondingly the Boussinesq and rigid-lid approximations will be made. We take $\Delta\rho \geqslant 0$ and $f \geqslant 0$, so that the current flows along the upper boundary and right-hand wall of the channel, but note that no generality is lost through this choice under the Boussinesq and rigid-lid approximations. It is assumed that the flow relative to the nose and the speed of propagation c_f are steady. The calculation is to be carried out in a frame of reference translating with the nose of the gravity current, which will be called the steady frame; the non-translating frame will be called the rest frame. Away from the nose, it is supposed that there exists a region where the interface and flow become parallel to the along-channel direction and conditions are hydrostatic and geostrophic. This region will be referred to as the *control point*. The flow may be non-hydrostatic and ageostrophic in a control volume V connecting the hydrostatic geostrophic regions at the control point and the ambient fluid far ahead of the gravity current.

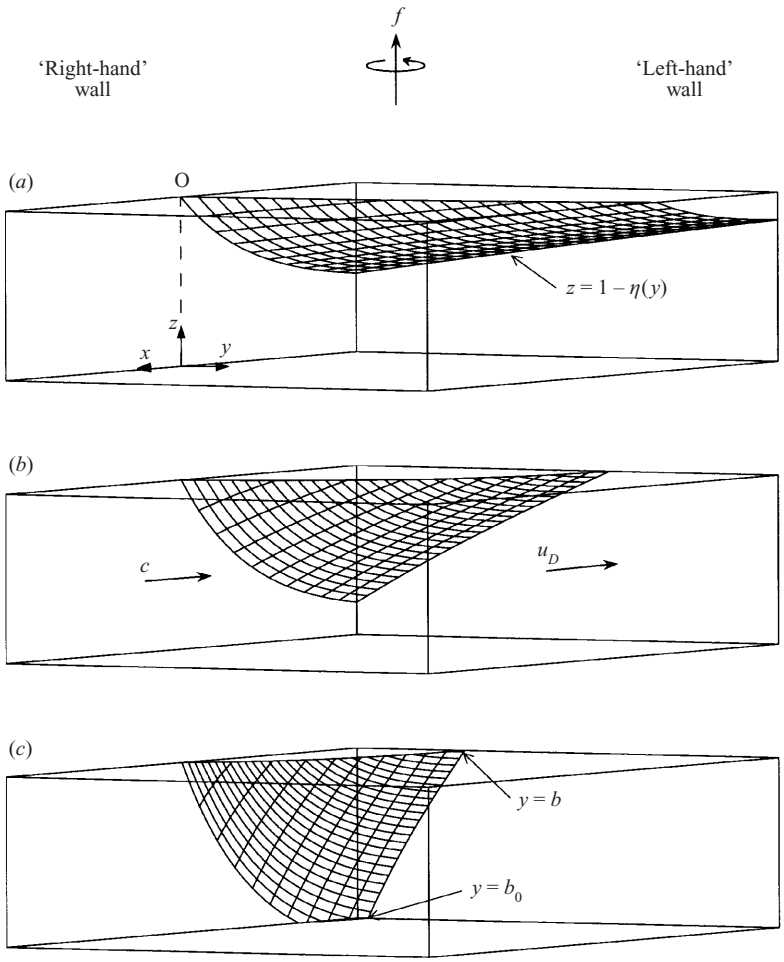

FIGURE 1. The three possible flow geometries viewed from 'upstream' in the steady frame. (*a*) Case A (low rotation): the current extends across the complete width of the channel. (*b*) Case B (moderate rotation): the current separates from the left-hand wall and the downstream front outcrops on the upper boundary at $y = b$. (*c*) Case C (strong rotation): the depth of the current at the right-hand wall reaches the full depth and the front outcrops on the lower boundary at $y = b_0$.

Benjamin (1968) supposed that the depth of the gravity current asymptotes slowly to a constant value at the control point, but there is no particular need for this assumption. Indeed, since there can be non-hydrostatic ageostrophic motion in V, the control point need only be a local extremum in the depth and width of the current and need not necessarily be a large distance from the nose. However, we may suppose, as is the case in the non-rotating case, that the flow at the control point is supercritical, in the sense that waves generated downstream (with respect to the ambient flow) are not able to reach the control point and modify the flow there, so that conditions at that point remain steady and continue to dictate the propagation of the front. Nof (1987) considered the control point to be a distance of the order of a deformation radius from the nose, but there is no need for this restriction either, since the shape of the interface ahead of the control point is governed by the ageostrophic dynamics in that region.

To obtain the governing equations for the flow in the steady frame, take right-

handed Cartesian coordinates (x, y, z) with respective units vectors $\boldsymbol{i}$, $\boldsymbol{j}$ and $\boldsymbol{k}$, as shown in figure 1. The equations expressing conservation of momentum, volume and PV are, then, respectively:

$$\boldsymbol{u}\cdot\nabla\boldsymbol{u} + f\boldsymbol{k}\times\boldsymbol{u} = -\rho_a^{-1}\nabla p - fc\boldsymbol{j} + \delta_{i1}g'\boldsymbol{k}, \tag{2.1}$$

$$\nabla\cdot\boldsymbol{u} = 0, \tag{2.2}$$

$$\boldsymbol{u}\cdot\nabla q = 0. \tag{2.3}$$

Here, $\boldsymbol{u} = (u, v, w)$ is the velocity, $f = \frac{1}{2}\Omega$ is the Coriolis frequency, $g' \equiv g\Delta\rho/\rho_a$ is the reduced gravity, δ_{ij} is the Kronecker delta with $i = 1$ and $i = 2$ labelling the gravity current and ambient fluid layers, respectively, and $p = p_T + \rho_a(gz - \frac{1}{2}\Omega^2 r^2)$ is the modified pressure (henceforth simply 'the pressure') in which p_T is the total pressure and r the distance from the rotation axis. Without loss of generality, we take $p = 0$ at the forward stagnation point at the nose (the point O in figure 1). In (2.3), q is the Ertel potential vorticity defined by

$$q = (f\boldsymbol{k} + \boldsymbol{\omega})\cdot\nabla Z(\boldsymbol{x}), \tag{2.4}$$

where $\boldsymbol{\omega} \equiv \nabla\times\boldsymbol{u}$ is the relative vorticity and $Z(\boldsymbol{x})$ is the upstream height of a material surface at downstream position $\boldsymbol{x}$.†

The new term that appears in the momentum equation (2.1) is the second term on the right-hand side. This is a fictitious force experienced everywhere in the steady frame because the whole frame of reference is translating in a rotating system, i.e. it is the Coriolis force experienced by the whole frame of reference in the rest frame. This force is not part of the Coriolis force experienced by the flow in the steady frame and will be called the *force of translation* to make this distinction clear.

In the ambient fluid far upstream of the nose and at the downstream control point, the flow is parallel, and, since the flow there is geostrophic, it is also depth independent (by the Taylor–Proudman theorem), so that

$$\boldsymbol{u} = (u(y), 0, 0). \tag{2.5}$$

It follows, then, from (2.4), that in these regions q is given by

$$q = q^g(y) \equiv \frac{H(f - \mathrm{d}u/\mathrm{d}y)}{h_i(y)}, \tag{2.6}$$

where $h_i(y)$ is the relevant layer depth and the superscript g indicates evaluation in a geostrophic region of the flow.

It is convenient to use the non-dimensional variables

$$\hat{x} = x/B, \quad \hat{y} = y/B, \quad \hat{z} = z/H, \tag{2.7a–c}$$

$$\hat{\boldsymbol{u}} = \boldsymbol{u}/(g'H)^{1/2}, \quad \hat{c} = c/(g'H)^{1/2}, \tag{2.7d, e}$$

$$\hat{p} = p/(\rho_a g'H), \quad \hat{q} = q(f/H)^{-1}, \quad \eta_i = h_i/H, \tag{2.7f–h}$$

which are $O(1)$ in the two-layer non-rotating case. Henceforth dropping the hats, (2.1) and (2.6) become

$$\boldsymbol{u}\cdot\nabla\boldsymbol{u} + W\boldsymbol{k}\times\boldsymbol{u} = -\nabla p - Wc\boldsymbol{j} + \delta_{i1}\lambda_H^{-1}\boldsymbol{k}, \tag{2.8}$$

† Except where ambiguity arises, the terms upstream and downstream will be used with reference to the direction of the ambient flow in the steady frame.

$$q^g(y) = \frac{(1 - W^{-1}\,\mathrm{d}u/\mathrm{d}y)}{\eta_i(y)}, \tag{2.9}$$

where $\nabla \equiv (\partial/\partial x, \partial/\partial y, \lambda_H^{-1}\partial/\partial z)$, $\lambda_H \equiv H/B$ and $W \equiv fB/(g'H)^{1/2}$ is the parameter expressing the strength of the background rotation defined in (1.2), which here plays the role of an inverse Rossby number. It will be seen later that λ_H drops out of the calculation, and so the problem is governed solely by W.

When the solution is obtained in § 3, it will be found that three types of across-channel structure are possible according to the value of W, labelled Cases A, B and C and shown in figure 1. In Case A (small W; low rotation), the current extends across the complete width of the channel at the control point; in Case B (moderate W; intermediate rotation), the current separates from the left-hand wall at the control point and the interface outcrops on the upper boundary at position $y = b$; in Case C (large W; strong rotation), the depth of the current at the right-hand wall is the complete depth, and the interface outcrops on both the upper and lower boundaries, at positions $y = b$ and $y = b_0$, respectively. The geometry considered by Nof (1987) corresponds to that of Case B. In order to write the governing equations in a single form valid for all three cases, it will be taken that for

$$\text{Case A} : b = 1, \quad b_0 = 0, \tag{2.10a}$$

$$\text{Case B} : \eta(b) = 0, \quad 0 \leqslant b \leqslant 1, \quad b_0 = 0, \tag{2.10b}$$

$$\text{Case C} : \eta(b) = 0, \quad \eta(b_0) = 1, \quad 0 \leqslant b_0 < b \leqslant 1, \tag{2.10c}$$

where $\eta = \eta_1(y)$ is the depth of the current at the control point.

As discussed in § 1, the aim of the calculation is to determine the speed of propagation of the nose and the structure of the flow at the control point. The first stage (§ 2.1) is to integrate (2.8) and (2.9) to obtain general solutions for the upstream and downstream flow. Then, as in Benjamin's (1968) calculation, boundary conditions fixing the values of the constants of integration in these solutions are provided by writing down equations in terms of the upstream and downstream fields expressing conservation of (i) energy (Bernoulli's theorem), (ii) volume, and (iii) momentum (the flow-force balance). These equations will be called the constraint equations and are derived in § 2.2.

2.1. *Upstream and downstream flow structure*

In the upstream and downstream regions, (2.8) reduces to the hydrostatic and geostrophic relations:

$$\frac{\partial p}{\partial z} = \delta_{i1}, \tag{2.11}$$

$$\frac{\partial p}{\partial y} = -W(u(y) - c). \tag{2.12}$$

The flow in the steady frame is not strictly geostrophic, as the across-channel pressure gradient is balanced by the combined effect of the steady-frame Coriolis force and the force of translation. In order to draw an analogy with the gravitational term, which will prove helpful later, we will refer to the terms on the right-hand side of (2.12) collectively as the *rotational buoyancy*.

Upstream in the ambient fluid

$$u_a = -c, \tag{2.13}$$

and from (2.12) the pressure is constant, p_u, say. Downstream at the control point,

integration of (2.11)–(2.12) gives the pressure within the gravity current as

$$p_c(y,z) = (z-1) - P(y), \tag{2.14}$$

where the subscript c indicates evaluation within the gravity current, and

$$P(y) = -p_0 + Wcy + W\int_0^y u_c(s)\,\mathrm{d}s, \tag{2.15}$$

is the part of the pressure variation balancing the rotational buoyancy forces acting on the current, less the constant of integration $p_0 = p_c(0,1)$. The pressure is continuous at the interface, and so evaluating (2.14) at $z = 1-\eta(y)$ gives

$$p_D(y) = -\eta(y) - P(y), \quad y \in [b_0, b], \tag{2.16}$$

where the subscript D indicates evaluation in the downstream ambient fluid region.

An assumption must now be made regarding the form of the velocity profile within the gravity current $u_c(y)$. This may be imposed either by specifying $u_c(y)$ directly, or by specifying the PV distribution. As discussed in § 1, here we will consider the simplest case, of zero font-relative velocity

$$u_c = 0, \tag{2.17}$$

for which the last term in (2.15) vanishes identically, and, since there is no x-dependence within the gravity current, $p_0 = 0$, the value at the forward stagnation point. Hence

$$P(y) = Wcy. \tag{2.18}$$

For convenience, let the flow in the ambient fluid at the control point

$$u(y) = -u_D, \tag{2.19}$$

with it being supposed that $u_D \geqslant c > 0$, since we exclude the possibility of stagnant or recirculating regions in the ambient fluid. Substituting (2.16) with (2.18) into (2.12) gives

$$\frac{\mathrm{d}\eta}{\mathrm{d}y} = -Wu_D(y), \tag{2.20}$$

and use of (2.9), with $q_a = 1$ given by the upstream conditions and $\eta_2 = 1-\eta$, gives

$$\frac{\mathrm{d}u_D}{\mathrm{d}y} = -W\eta(y). \tag{2.21}$$

The general solution to (2.20) and (2.21) for $y \in [b_0, b]$ is

$$\eta(y) = \eta_0 \cosh W(y-b_0) - u_0 \sinh W(y-b_0), \tag{2.22}$$

$$u_D(y) = u_0 \cosh W(y-b_0) - \eta_0 \sinh W(y-b_0), \tag{2.23}$$

where $\eta_0 = \eta(b_0)$ and $u_0 = u_D(b_0)$ are the constants of integration. The values of b and b_0 are given in terms of η_0 and u_0 by the geometrical constraints (2.10), which for Cases B and C give

$$b - b_0 = W^{-1}\mathrm{arctanh}(\eta_0/u_0), \tag{2.24}$$

and for Case C

$$\eta_0 = 1. \tag{2.25}$$

In the ambient fluid region beyond the edge of the current $y \in [b, 1]$, henceforth the *free stream*, there is no shear, by virtue of (2.21), and hence $u_D = U$, say, a constant. Although it is not necessary for u_D to be continuous on $y = b$ for kinematic

reasons, it will be shown later that energy conservation requires u_D to be continuous everywhere, and hence, from (2.23),

$$U = u_0 \cosh W(b - b_0) - \eta_0 \sinh W(b - b_0). \tag{2.26}$$

Finally, the pressure in the free stream is obtained by integrating (2.12), with boundary condition at $y = b$ provided by (2.16) and (2.18), to obtain

$$p_D(y) = W(U - c)(y - b) - Wcb, \quad y \in [b, 1]. \tag{2.27}$$

2.2. *The constraint equations*

2.2.1. *Conservation of energy*

For the flow in the steady frame, Bernoulli's theorem is

$$\mathrm{B} \equiv \tfrac{1}{2}|\boldsymbol{u}|^2 + p + Wcy = \text{constant on streamlines}, \tag{2.28}$$

as may be obtained from (2.8) in the usual way (see also Stern *et al.* 1982). The new term, arising from the background rotation, is the last term on the right-hand side. This is the potential energy of a fluid element owing to its position in the field of the force of translation. Its action is analogous to that of the gravitational potential energy term; e.g. positive movement across the channel (towards the left-hand wall) requires work to be done against the force of translation, and so leads to a gain in rotational potential energy. Coriolis forces do not contribute to B since they act in the direction perpendicular to the streamlines, and, therefore, only influence the energy of fluid elements through their effect on the pressure field.

At the stagnation point at the nose, $u = p = 0$ and hence, from (2.28), $\mathrm{B} = 0$. Then applying (2.28) along the ambient fluid streamline following the right-hand wall to the stagnation point gives

$$p_u = -\tfrac{1}{2}c^2, \tag{2.29}$$

as in the non-rotating case, this being simply a dynamic pressure drop relative to the nose produced by the upstream ambient flow. This expression eliminates one of the four unknown constants of integration, p_u say.

Substituting (2.29) into (2.28) gives

$$\mathrm{B}_u(y) = Wcy, \tag{2.30}$$

showing that the only variation in B upstream comes from the rotational potential energy term. For the downstream flow, let $\mathrm{Y}(y)$ denote the upstream across-channel position of streamlines at downstream position y. Then applying (2.28) along ambient streamlines connecting the upstream and downstream locations and using (2.30) gives the downstream Bernoulli function

$$\mathrm{B}_D(y) \equiv \tfrac{1}{2}u_D^2 + p_D + Wcy = Wc\mathrm{Y}(y). \tag{2.31}$$

Note that streamlines following the upper boundary do not pass directly around the current, but are subducted along the line of the outcropping front. From (2.31) it is seen that $u_D(y)$ must be continuous everywhere in the energy conserving flow, as was asserted in § 2.1, since p_D and $\mathrm{Y}(y)$ must be continuous on kinematic grounds.

To examine the contribution of the various terms in (2.31), let

$$\Delta\mathrm{Y}(y) \equiv y - \mathrm{Y}(y), \tag{2.32}$$

the displacement of streamlines from their upstream position. Then, substituting for the downstream ambient fluid pressure, (2.16), (2.18) and (2.27), (2.31) may be

re-written

$$\tfrac{1}{2}u_D^2 = \begin{cases} \eta(y) + Wcy - Wc\Delta\mathrm{Y}(y), & y \in [b_0, b], \\ Wcy - WU(y-b) - Wc\Delta\mathrm{Y}(y), & y \in [b, 1]. \end{cases} \tag{2.33a,b}$$

This equation shows that the action of the rotational buoyancy forces is analogous to that of gravity, in the sense that both effects decrease the ambient fluid pressure at the control point, and hence accelerate the downstream ambient flow. The relative magnitudes of the momentum inputs from these two sources will be considered in § 3.5. Equation (2.33) also shows that the changes in the ambient fluid pressure produced by the rotational buoyancy forces acting on the gravity current are essential in establishing the types of flow structure envisaged in figure 1. For example, in the absence of this energy input (e.g. as would be the case for a current of zero density) Cases B and C could not be realized ($\eta(b) = 0$ in (2.33*a*)) without either $\Delta\mathrm{Y}(b)$ becoming negative or $U = 0$, which are both unphysical situations in the context of the theory.

In order to make use of (2.33), values of $\Delta\mathrm{Y}$ must be known *a priori*. This is the case only for streamlines at the boundaries of the ambient fluid, for which

$$\Delta\mathrm{Y}(b_0) = b_0, \quad \Delta\mathrm{Y}(1) = 0, \tag{2.34}$$

and hence, from (2.33),

$$\tfrac{1}{2}u_0^2 = \eta_0, \tag{2.35}$$

$$\tfrac{1}{2}U^2 = \eta(1) + Wc - WU(1-b). \tag{2.36}$$

Through the general solution for the downstream flow structure, these equations give two independent equations for the three remaining unknowns: c, u_0 and η_0. The first, (2.35), gives a simple relation between u_0 and η_0 which is unchanged from that in the non-rotating case. The modification to this energy balance from the across-channel pressure gradients induced by the rotational buoyancy forces acting across the span of the channel is given by (2.36).

2.2.2. *Continuity of volume flux*

There are two remaining conditions to be applied – conservation of volume and momentum in V – but only one further independent constraint is required to close the problem. Seemingly then the problem is overspecified. This is not the case, however, since the information regarding volume conservation has in fact already been included implicitly in the formulation through the conditions of PV and energy conservation. To see this, observe that differentiation of the definition of the Bernoulli function B in (2.28) and use of the geostrophic equation (2.12) and the definition of q^g in (2.9) gives

$$uq^g\eta_i = -W^{-1}\frac{\mathrm{dB}}{\mathrm{d}y}. \tag{2.37}$$

The Bernoulli function, therefore, acts as a streamfunction for the downstream PV flux. This relationship has been discussed by Gill (1982) and in a more general context by Schär (1993). Since $q = 1$ in the ambient fluid, the PV and volume fluxes are synonymous, and hence using (2.37), together with (2.31) and (2.34), it follows that the downstream volume flux

$$\int_{b_0}^{1} u_D(1-\eta)\,\mathrm{d}y = W^{-1}(\mathrm{B}_D(1) - \mathrm{B}_D(b_0)) = c(\mathrm{Y}(1) - \mathrm{Y}(b_0)) = c, \tag{2.38}$$

which is the upstream volume flux. Hence, the conditions of PV and energy conservation are sufficient to ensure volume conservation in the ambient fluid.

2.2.3. *Conservation of bulk momentum*

The final condition required is that of bulk momentum conservation in V. We wish to express this condition as the conservation of some across-channel integrated quantity, e.g. a 'flow-force', that is conserved between the upstream and downstream locations. Nof (1987) derived such an expression for a hydrostatic flow, and then argued that the same result should hold when non-hydrostatic regions exist in V. Although the result obtained is correct, as will be shown below, this heuristic argument is not necessarily convincing, and the mathematics of his derivation are also somewhat involved. Here, we offer a simpler derivation which does not require the hydrostatic assumption to be made.

Integration of the momentum equation (2.8) over V and use of the divergence theorem (e.g. Batchelor 1967, § 3.2) gives:

$$\int_{\partial V} (\boldsymbol{u}(\boldsymbol{u}\cdot\boldsymbol{n}) + p\boldsymbol{n})\,\mathrm{d}A + W\int_V (\boldsymbol{k}\times\boldsymbol{u})\,\mathrm{d}V = -Wc\boldsymbol{j}\int_V \mathrm{d}V + \boldsymbol{k}\int_{V_c}\mathrm{d}V, \tag{2.39}$$

where ∂V is the boundary of V with outward normal $\boldsymbol{n}$ and V_c is the part of V occupied by the gravity current. The first term on the left-hand side is familiar from the non-rotating case, this being the non-rotating flow-force. The two body-force terms on the right-hand side, the total gravitational buoyancy and translational forces acting on V, are not of interest here since they do not act in the along-channel direction. The second term on the left-hand side, the volume integral of the Coriolis forces acting in V, does have an along-channel component induced by across-channel motion, and in order for (2.39) to be useful this term must be expressed in terms of surface integrals across the upstream and downstream regions. Here, such a decomposition may be made by virtue of the incompressibility condition (2.2), which allows the velocity to be written $u_i = \partial(x_i u_j)/\partial x_j$, where suffix notation has been used, and therefore $[\boldsymbol{k}\times\boldsymbol{u}]_i = -\epsilon_{ij3}u_j = -(\epsilon_{ij3}x_j u_k)_{,k}$, where ϵ_{ijk} is the alternating tensor. From the divergence theorem, therefore,

$$\int_V (\boldsymbol{k}\times\boldsymbol{u})\,\mathrm{d}V \equiv \int_V (-v\boldsymbol{i}+u\boldsymbol{j})\,\mathrm{d}V = \int_{\partial V}(-y\boldsymbol{i}+x\boldsymbol{j})(\boldsymbol{u}\cdot\boldsymbol{n})\,\mathrm{d}A. \tag{2.40}$$

Substituting this expression into (2.39) and taking the x-component of the resulting expression shows that the 'flow-force'

$$S \equiv \int_0^1 \left(u_i^2\eta_i + \int_0^1 p\,\mathrm{d}z - Wyu_i\eta_i\right)\mathrm{d}y, \tag{2.41}$$

is equal at the upstream and downstream locations. This is equivalent to the expression obtained by Nof (1987), and verifies his heuristic argument. The form of the Coriolis force term (the last term on the right-hand side of (2.41)) arises because the difference in the value of this term between any pair of geostrophic upstream and downstream locations, at equal y, gives the total across-channel flow across a vertical plane connecting these locations, times W, and hence the total along-channel Coriolis force integrated across that plane (this may be seen by integrating this term once by parts; see Hacker (1996) for further discussion).

For the upstream flow, substituting (2.13) and (2.29) into (2.41) gives:

$$S_U = \tfrac{1}{2}c(c+W). \tag{2.42}$$

For the downstream flow, it is shown in Appendix B that use of the general solution for the downstream flow structure together with the Bernoulli constraints gives:

$$S_D = \tfrac{1}{2}c(U+W) - \tfrac{1}{2}b_0 - \tfrac{1}{12}W^{-1}(u_0^3 - U^3). \tag{2.43}$$

Hence, equating the flow-force upstream and downstream gives

$$6W(c(U-c) - b_0) = u_0^3 - U^3, \tag{2.44}$$

which, through the general solution for the downstream fields, gives a third equation for the three remaining unknown parameters, and thereby closes the problem.

3. The two-layer solution

In this section we solve the constraint equations (2.35)–(2.36) and (2.44) for the two-layer case in which $\eta_0 = O(1)$. The solutions for the three case geometries are obtained in turn in §§ 3.1–3.3, and are then discussed in § 3.4.

3.1. *The solution for Case A*

For Case A, the constraint equations (2.35)–(2.36) and (2.44) are

$$\tfrac{1}{2}u_0^2 = \eta_0, \tag{3.1}$$

$$Wc = \tfrac{1}{2}u_D^2(1) - \eta(1), \tag{3.2}$$

$$6Wc(u_D(1) - c) = u_0^3 - u_D^3(1). \tag{3.3}$$

Substituting $\eta(1)$ and $u_D(1)$ from (2.22)–(2.23) into (3.3) and use of (3.1)–(3.2) gives a single equation for u_0, which is a sixth-order polynomial with coefficients that are transcendental functions of W. It was not possible to determine a closed-form solution to this equation, and the roots were determined numerically. Graphical inspection shows that there are two non-zero solution branches $u_0(W)$. One of these has $u_0(W) < 0$, and so is unphysical. The other has $u_0(W) > 0$ and connects to Benjamin's non-rotating solution in the limit $W \to 0$ (see § 3.1.1 below). An efficient numerical procedure to determine this solution branch is to iterate (3.3) on u_0 with W fixed (e.g. using Newton–Raphson iteration) with $c(u_0, W)$, $\eta(1; u_0, W)$ and $u_D(1; u_0, W)$ given implicitly by (3.1)–(3.2) and (2.22)–(2.23). The first iteration may be carried out for W close to zero, with Benjamin's non-rotating solution used as the first guess, and then W incremented and the root from the preceding iteration used as the next first guess, and so on, until the end of the regime is signalled by the vanishing of the depth of the gravity current at the left-hand wall, i.e. $\eta(1) = 0$, which occurs at $W = W_A = 0.6710$.

The solution obtained in this way is shown in figure 2. Also shown is the $O(W)$ asymptotic solution, obtained in § 3.1.1 below. All three variables increase in line with the linear asymptotic solution, although do show some curvature. An intriguing feature is the apparent intersection of the curves for c and u_0 at the endpoint of the solution branch; the implied solution $(u_0 - \frac{1}{2}) = c = W$ at $W = W_A$ is in fact only approximate, but is accurate to ± 0.001. There appears to be no obvious reason why this should be the case.

3.1.1. $O(W)$ *asymptotic solution*

Although it was not possible to obtain a closed form solution to (3.1)–(3.3), it is straightforward to obtain the asymptotic solution for small W. This is instructive

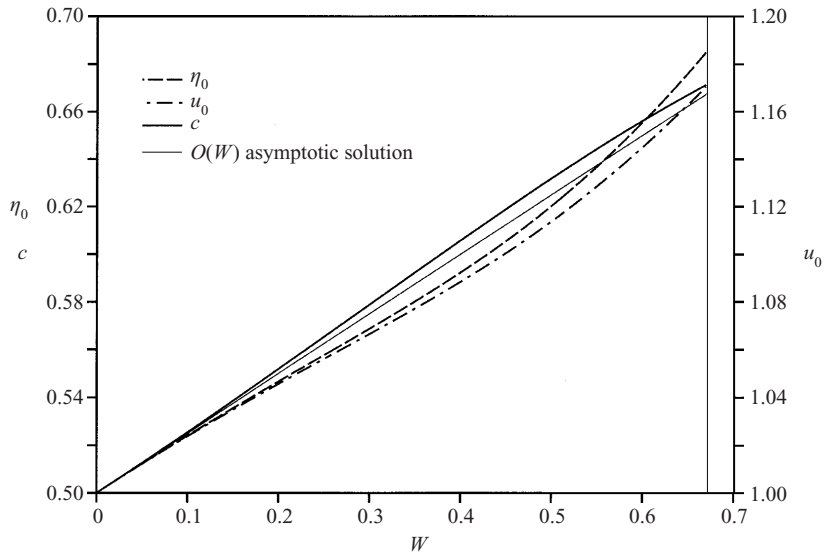

FIGURE 2. The Case A solution for the model variables u_0, η_0 and c, plotted as a function of W, obtained from the numerical solution of (3.1)–(3.3). Also shown is the $O(W)$ asymptotic solution given by (3.8).

and indicates how the model equations behave as $W \to 0$. Expand the dependent variables as regular power series in W

$$u_0 = u_0^* + u_1 W + u_2 W^2 + O(W^3),$$
$$\eta_0 = \eta_0^* + \eta_1 W + \eta_2 W^2 + O(W^3),$$
$$c = c_0 + c_1 W + c_2 W^2 + O(W^3),$$

and balance terms in (3.1)–(3.3) at given orders of W in the usual way.

At $O(1)$, (3.1) and (3.2) both reduce to

$$\eta_0^* = \tfrac{1}{2} u_0^{*2}, \tag{3.4}$$

which is the non-rotating Bernoulli equation; this is to be expected, since for $W = 0$ there is no across-channel dependence. The $O(1)$ terms in (3.3) cancel exactly, so this equation gives no information at this order.

At $O(W)$, (3.1)–(3.3) give, respectively,

$$\eta_1 = u_0^* u_1, \tag{3.5a}$$

$$c_0 = u_0^*(1 - \eta_0^*) + u_0^* u_1 - \eta_1, \tag{3.5b}$$

$$2c_0(u_0^* - c_0) = u_0^{*2}\eta_0^*. \tag{3.5c}$$

Although the first two equations involve higher-order terms, the last two terms in (3.5b) vanish by virtue of (3.5a), leaving

$$c_0 = u_0^*(1 - \eta_0^*), \tag{3.5d}$$

which is the non-rotating ambient fluid volume-flux conservation equation, and indicates that (2.38) remains valid in the limit $W \to 0$, even though the derivation of this equation involved division by W. Equation (3.5c) is less obviously equivalent to the non-rotating flow-force balance, because of the manipulations involved in the

derivation of (2.44), but it is straightforward to confirm that the solution to (3.4) and (3.5*c–d*) is

$$\eta_0^* = \tfrac{1}{2}, \quad u_0^* = 1, \quad c_0 = \tfrac{1}{2}, \tag{3.6}$$

which is Benjamin's non-dissipative two-layer solution for the non-rotating case. This confirms that the model equations reduce smoothly to those for the non-rotating case in the limit $W \to 0$.

To obtain the $O(W)$ perturbations it is necessary to proceed to $O(W^2)$. Again, it is necessary to take the difference of the two Bernoulli equations (3.1) and (3.2) in order to eliminate the higher-order terms appearing in these expressions, and to make use of the Bernoulli equation at the right-hand wall from the proceeding order, (3.5*a*). Together with the $O(W)$ balance from (3.3) and the leading-order solution (3.6), this gives the equations of energy, volume and flow-force conservation, respectively, for the $O(W)$ perturbations as

$$\eta_1 = u_1, \quad c_1 = \tfrac{1}{2}u_1 - \eta_1 + \tfrac{3}{8}, \quad 0 = \eta_1 - \tfrac{1}{4}, \tag{3.7a–c}$$

which have solution $\eta_1 = u_1 = c_1 = \frac{1}{4}$.

To summarize, the asymptotic solution accurate to $O(W^2)$ is

$$c \sim \tfrac{1}{2} + \tfrac{1}{4}W, \quad \eta_0 \sim \tfrac{1}{2} + \tfrac{1}{4}W, \quad u_0 \sim 1 + \tfrac{1}{4}W, \tag{3.8a–c}$$

and, from (2.22) and (2.23),

$$\eta(y) \sim \tfrac{1}{2} + W(\tfrac{1}{4} - y), \quad u_D(y) \sim 1 + \tfrac{1}{2}W(\tfrac{1}{2} - y). \tag{3.9a,b}$$

From figure 2 it can be seen that (3.8) captures the behaviour of the numerical solution very well.

The small–W analysis above provides physical insight into the initial effects of the rotation. First, considering the momentum equation at $O(W^2)$, (3.7*c*), the terms involving c_1, u_1 and the higher-order perturbations vanish, and therefore this equation is decoupled from the other constraint equations at this order, i.e. the $O(W)$ depth perturbation is set independently of the other perturbations. Physically, this may be viewed as a consequence of the movement of fluid across the channel produced by the Coriolis force exerted on the $O(1)$ along-channel flow. Secondly, considering the Bernoulli equation at the right-hand wall (3.7*a*), since c_1 does not appear in this equation (as is true at all orders) it follows that the $O(W)$ downstream flow perturbation is set independently of the upstream perturbation. The increase in the front speed may be seen, therefore, to be a consequence of the fact that the perturbed downstream flow draws an increased volume flux, and hence the upstream volume flux c must increase accordingly.

3.2. *The solution for Case B*

For Case B, the constraint equations (2.35)–(2.36) and (2.44) are

$$\tfrac{1}{2}u_0^2 = \eta_0, \tag{3.10}$$

$$Wc = \tfrac{1}{2}U^2 + W(1-b)U, \tag{3.11}$$

$$6Wc(U-c) = u_0^3 - U^3, \tag{3.12}$$

where from (2.26) and (2.24)

$$U = u_0 \cosh Wb - \eta_0 \sinh Wb, \tag{3.13}$$

$$Wb = \operatorname{arctanh}(\eta_0/u_0). \tag{3.14}$$

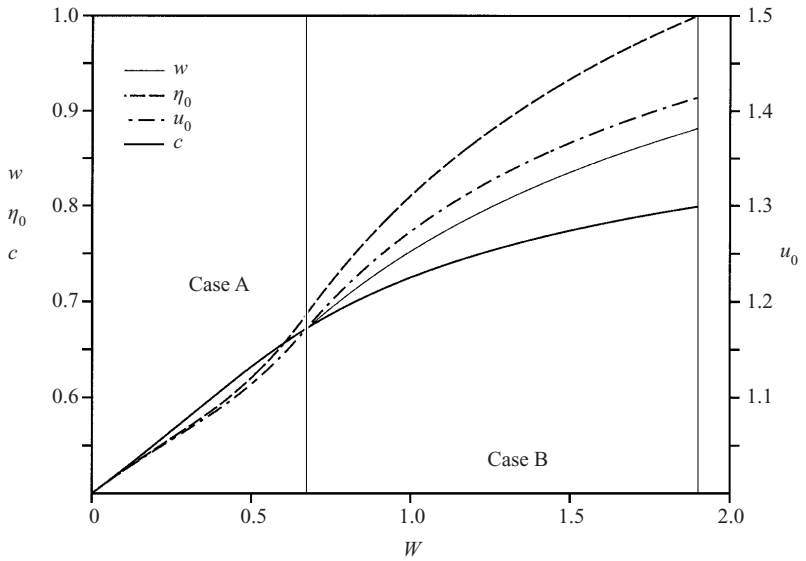

FIGURE 3. The Case B solution for the model variables u_0, η_0, c and $w = Wb$, given by (3.16)–(3.17) and (3.19)–(3.20) plotted as a function of W, together with the Case A solution.

In this case, a closed-form solution may be obtained in terms of the additional variable

$$w \equiv Wb, \tag{3.15}$$

which is the width of the current in terms of deformation radii R. From (3.10) and (3.14)

$$u_0 = 2\tanh w, \tag{3.16}$$

$$\eta_0 = 2\tanh^2 w, \tag{3.17}$$

and then from (3.13)

$$U = 2\,\mathrm{sech}\, w \tanh w. \tag{3.18}$$

Substituting these into (3.11) and (3.12) and solving gives:

$$c = \frac{2\,\mathrm{sech}^2 w \tanh^2 w(\cosh^3 w - 1)}{3(w - \mathrm{sech}\, w \tanh w)}, \tag{3.19}$$

$$W = \frac{(w - \mathrm{sech}\, w \tanh w)^2}{w - \frac{1}{3}\,\mathrm{sech}\, w \tanh w(2 + \cosh^3 w)}. \tag{3.20}$$

All that remains is to determine the physical branch of the $w - W$ relationship (3.20). Graphical inspection of this relationship, with the requirements that $0 \leqslant b \leqslant 1$ and $0 \leqslant \eta_0 \leqslant 1$ for $W \geqslant 0$, indicates that there is only one physical solution branch. This connects smoothly to the Case A solution at $w = W = W_A$ and thereafter has w increasing with W, with the endpoint of the regime, signalled by $\eta_0 = 1$, occurring at

$$w = w_B \equiv \mathrm{arctanh}\,(2^{-1/2}) = 0.881, \tag{3.21}$$

which corresponds to $W = W_B = 1.898$.

The solution as a function of W is shown in figure 3. All the variables continue to increase, although at a decreasing rate. It is also evident that the solution is smooth at the Case A–B transition. As discussed above, the Case B geometry was

that considered by Nof (1987). His zero PV solution has very similar properties to that shown in figure 3, although the onset and endpoint of the Case B geometry occur at slightly smaller values of W. We will make more detailed comparisons with Nof's solution in Part 2, where cases of constant PV within the gravity current are considered. The values of b and η_0 given by the solution here at $W = 1.80$ are also quite similar to those in the numerical simulation of Wang (1985), discussed in § 1.2, although this is not true of the value of front speed c, which was somewhat less in Wang's simulation.

3.3. *The solution for Case C*

For Case C, the constraint equations (2.35)–(2.36) and (2.44) are

$$\tfrac{1}{2}u_0^2 = \eta_0, \tag{3.22}$$

$$Wc = \tfrac{1}{2}U^2 + W(1-b)U, \tag{3.23}$$

$$6Wc(U-c) = u_0^3 - U^3 + 6Wb_0, \tag{3.24}$$

where from (2.26) and (2.24)–(2.25), respectively,

$$U = u_0 \cosh W(b-b_0) - \eta_0 \sinh W(b-b_0), \tag{3.25}$$

$$W(b-b_0) = \operatorname{arctanh}(\eta_0/u_0), \tag{3.26}$$

$$\eta_0 = 1. \tag{3.27}$$

Again, it is possible to obtain a closed-form solution in this case. From (3.27) and (3.22)

$$u_0 = 2^{1/2}, \tag{3.28}$$

and hence from (3.26)

$$\delta \equiv W(b-b_0) = w_B, \tag{3.29}$$

given by (3.21), is a constant throughout Case C, this variable being the width of the region over which the interface slopes in terms of deformation radii R. It may be shown from (3.21) that $\cosh w_B = 2^{1/2}$ and $\sinh w_B = 1$ (e.g. use the identities $\sinh w_B \equiv (\coth^2 w_B - 1)^{1/2}$, $\cosh w_B \equiv (1 + \sinh^2 w_B)^{1/2}$). Hence, from (3.25) with (3.27)–(3.28),

$$U = 1, \tag{3.30}$$

also a constant throughout Case C.

Combining (3.23) and (3.24) and using (3.28)–(3.30) gives a quadratic for c, which has the single physical root

$$c = 1 - kW^{-1/2}, \tag{3.31}$$

where $k = (w_B - \frac{1}{3}(1 + 2^{1/2})) = 0.2768$. The other root has $c > U$ and does not satisfy ambient fluid volume conservation for $b_0 \leqslant b \leqslant 1$, $0 \leqslant \eta_0 \leqslant 1$.

3.4. *Properties of the solution*

Figures 4 and 5 show across-channel interface and velocity profiles, respectively, for various values of W. Note that the velocity profiles are shown relative to the rest frame coordinates. The interface profiles are approximately linear, although with some curvature. The velocity profiles show sharper curvature towards the right-hand wall at small to moderate values of W. At higher values of W, a region of relatively intense shear develops beneath the current at the right-hand wall.

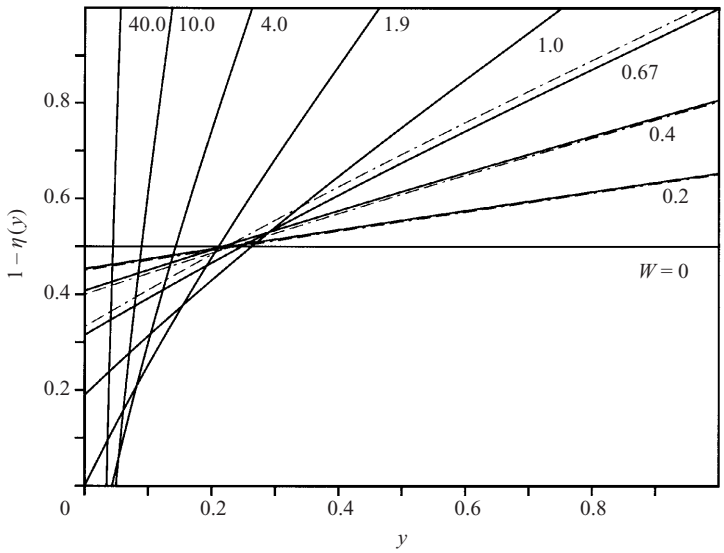

FIGURE 4. Downstream interface profiles (viewed from upstream) for $W = 0.0, 0.2, 0.4, 0.67$ (the Case A–B boundary), 1.0, 1.9 (the Case B–C boundary), 4.0, 10.0 and 40.0. The dot-dashed lines for $W \leqslant 0.67$ show the approximate solution discussed in the text.

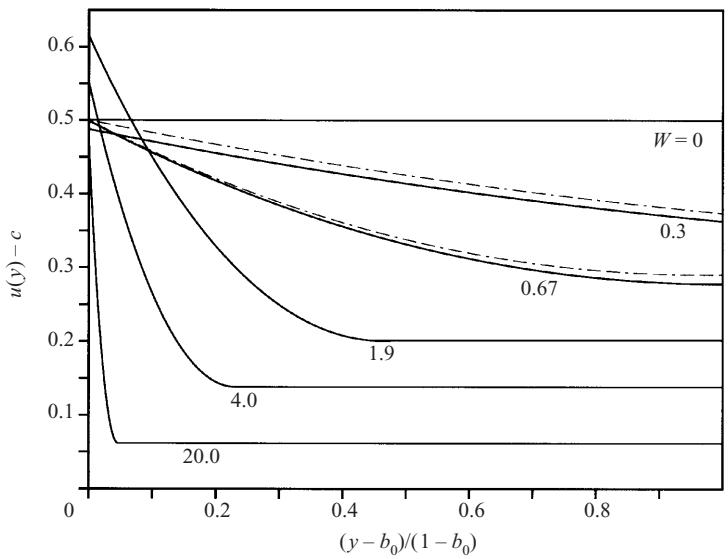

FIGURE 5. Downstream ambient fluid velocity profiles in the rest frame $u_D(y) - c$ (viewed from upstream) for $W = 0, 0.3, 0.67$ (the Case A–B boundary), 1.9 (the Case B–C boundary), 4.0 and 20.0. The dot-dashed lines for $W \leqslant 0.67$ show the approximate solution discussed in the text.

For Case A, an approximate solution obtained from (2.22)–(2.23) with values of c, u_0 and η_0 given by the $O(W)$ solution (3.8) is also shown in figures 4 and 5. This gives a better approximation to the profiles than the formally asymptotic expressions (3.9), since the $O(W^2)$ perturbations to the model parameters are relatively small (cf. figure 2).

For Cases B and C, analytic expressions for the profiles shown in figures 4 and

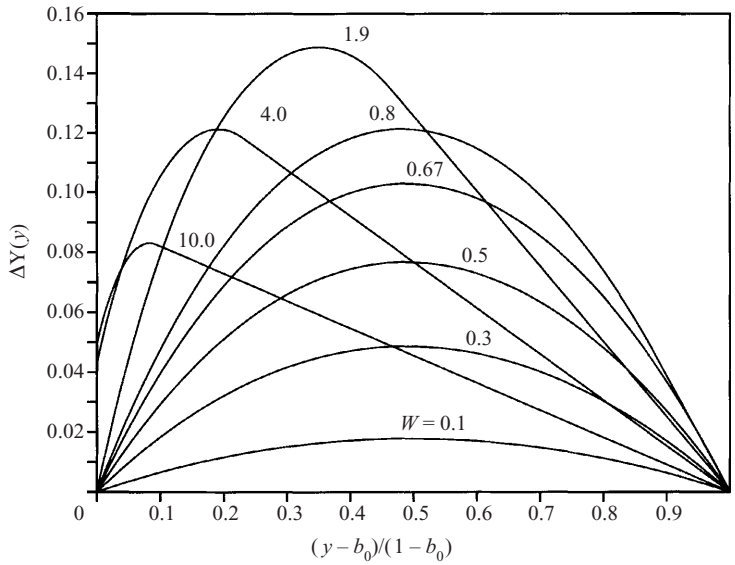

FIGURE 6. Downstream streamline displacement profiles $\Delta Y(y)$ (viewed from upstream) given by (2.33) for $W = 0.1, 0.3, 0.5, 0.67$ (the Case A–B boundary), 0.8, 1.9 (the Case B–C boundary), 4.0 and 10.0.

5 may be obtained by substituting (3.16)–(3.17) and (3.27)–(3.29) into (2.22)–(2.23), which, noting that $U = 1$ in Case C, gives:

$$\eta(y) = U \sinh W(b - y), \tag{3.32a}$$

$$u_D(y) = U \cosh W(b - y), \quad y \in [0, b]. \tag{3.32b}$$

In these cases, then, the interface and velocity profiles are simply given by sinh and cosh profiles, respectively, each centred on $y = b$ and with amplitude set by U. Since c asymptotes to $c = U = 1$ in the limit $W \to \infty$, by (3.30), the free stream becomes stagnant in the rest frame in this limit (cf. figure 5).

The streamline displacements $\Delta Y(y)$ obtained from the above solutions together with (2.33) are shown in figure 6. In Case A, values of ΔY increase everywhere across the channel, except at the walls where necessarily $\Delta Y = 0$; the profiles for this case appear to be very symmetric about $y = \frac{1}{2}$, but note the slight movement of the location of the maximum towards the right-hand wall. In Case B, the position of the maximum moves quite strongly towards the right-hand wall and increases in value, before starting to decrease at the onset of Case C.

The solutions for the width of the current on the upper and lower boundaries, b and b_0, respectively, are shown in figure 7. On the upper boundary, b decreases smoothly through Cases B and C, whereas on the lower boundary b_0 increases slowly from the start of Case C. The analytic expressions for these variables in Case C, obtained from (3.23), (3.29)–(3.31), are

$$b = kW^{-1/2} + \tfrac{1}{2}W^{-1}, \tag{3.33a}$$

$$b_0 = kW^{-1/2} + (\tfrac{1}{2} - w_B)W^{-1}, \tag{3.33b}$$

indicating that both widths decrease as $kW^{-1/2}$ as $W \to \infty$. Differentiation of (3.33b) indicates that b_0 reaches a maximum at $W = (2w_B - 1)^2/k^2 = 7.58$, thereafter

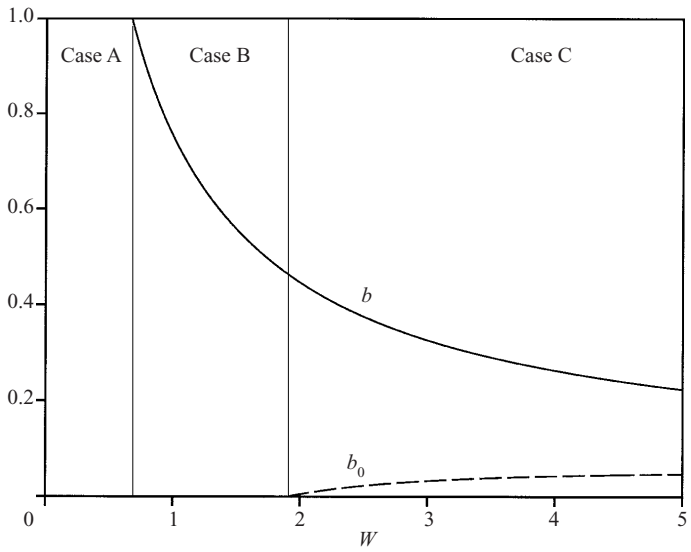

FIGURE 7. The width of the gravity current on the upper and lower boundaries, b and b_0, respectively, as functions of W.

decreasing. Note, from (3.33a), that $w = \frac{1}{2} + kW^{1/2}$ and so continues to increase with W.

The wall-depth based Froude number $c_0 = c_f(g'h_0)^{-1/2}$ is shown in figure 8. During Case A, c_0 increases by approximately 15%, reaching a maximum just before the onset of Case B. At the onset of Case C this quantity shows a gradient discontinuity, with thereafter $c_0 = c$, given by (3.31), since $h_0 = H$ in this case. Although the front speed c increases monotonically with W, the cross-sectional area of the current A_c decreases at a faster rate, with the result that the volume flux transported by the current (in the rest frame) decreases, as shown in figure 9.

3.5. *Flow-force diagnostics*

The non-monotonic variation of c_0 shown in figure 8 reflects the changing nature of the energy inputs into the system as the strength of the rotation increases, and, in particular, indicates that the increase in the front speed should not be attributed solely to the increase in the depth of the current at the right-hand wall. In order to examine the reasons for the increase in the front speed, consider how the various terms in the flow-force balance change as the strength of the rotation increases. We write the flow-force balance equation (as expressed by the x-component of the momentum integral (2.39)) as

$$F = P_U + P_B + P_C + C_a, \tag{3.34}$$

in which the sign convention adopted is such that positive terms act in the downstream direction, i.e. act to accelerate the ambient flow, and where:

$$\begin{aligned} F &= \int_{A_D} u_D^2 \,\mathrm{d}A - c^2, \\ &= \int_{b_0}^{1} (1-\eta) u_D^2 \,\mathrm{d}y - c^2, \end{aligned} \tag{3.35a}$$

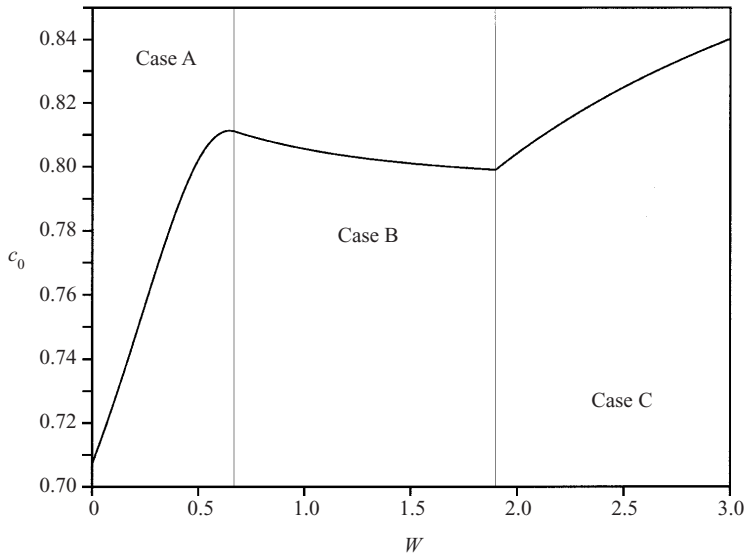

FIGURE 8. The wall-depth-based Froude number $c_0 = c_f/(g'h_0)^{1/2}$ as a function of W. Note that in Case C, $c_0 = c$, since $h_0 = H$, and therefore is given by (3.31).

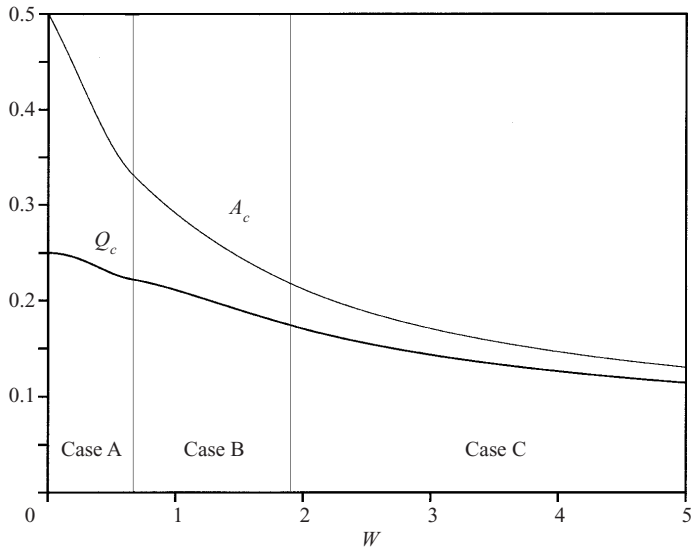

FIGURE 9. The cross-sectional area of the current A_c and the total volume flux $Q_c = cA_c$ carried by the gravity current in the rest frame as functions of W.

where A_D is the downstream ambient cross-section, is the increase in across-channel-integrated momentum flux between the upstream and downstream locations, i.e. the net force acting on the control volume V;

$$P_U = -\tfrac{1}{2}c^2, \tag{3.35b}$$

is the pressure force exerted on the upstream cross-section A_u owing to the dynamic pressure drop upstream;

$$P_B = \int_{A_c} (1-z)\,\mathrm{d}A - \int_{A_D} \eta(y)\,\mathrm{d}A,$$
$$= \tfrac{1}{2}b_0 + \int_{b_0}^{b} (\eta - \tfrac{1}{2}\eta^2)\,\mathrm{d}y, \tag{3.35c}$$

where A_c is the cross-section of the gravity current at the control point, is the increase in the pressure force exerted on the downstream cross-section owing to the buoyancy forces acting on the current;

$$P_C = \int_0^b Wcy\,\mathrm{d}y - \int_b^1 WU(y-b)\,\mathrm{d}y,$$
$$= \tfrac{1}{2}Wc - \tfrac{1}{2}WU(1-b)^2, \tag{3.35d}$$

is the pressure force exerted on the downstream cross-section owing to the rotational buoyancy forces acting on the gravity current and ambient flow; and

$$C_a = \int_{V_a} Wv(\boldsymbol{x})\,\mathrm{d}V,$$
$$= -\tfrac{1}{2}Wcb_0^2 - \int_{b_0}^1 Wc\Delta Y(y)\,\mathrm{d}y, \tag{3.35e}$$

where V_a is the ambient fluid part of the control volume and (2.40), (2.38) and (2.31) have been used in the second step, is the total along-channel Coriolis force. Each of the integrals may be evaluated analytically using the solutions for the various fields given above.

The variation of the terms in (3.34) with W is shown in figure 10. The total force F remains relatively constant, decreasing slightly as W increases. The terms on the right-hand side of (3.34), however, change quite significantly. The downstream pressure force due to gravitational buoyancy, P_B, decreases as the depth of the current increases, owing to the compensating effect of the reduction in cross-sectional area (cf. figure 10). In contrast, the downstream pressure force due to Coriolis forces, P_C, increases strongly with W, becoming the dominant positive term for larger W. At all levels of rotation, the total downstream pressure force $P_B + P_C$ exceeds the non-rotating value. Of the balancing negative terms, the magnitude of the upstream pressure force P_U increases in line with the front speed c according to (2.29) and the magnitude of the total along-channel Coriolis force C_a also increases as a result of the combined effect of the changing strength of the across-channel flow and the increasing value of W. The fact that F remains approximately constant indicates that the combined effect of these last two terms is to offset approximately the positive increase in the total downstream pressure force produced by the increase in P_C.

As shown in figure 9, the cross-sectional area of the ambient fluid at the control section increases with increasing W. Now, as a general principle, it becomes easier to drive fluid through a gap of given size as the size of the gap increases. Hence, given that the force on the control volume remains relatively constant, it is to be expected that the strength of the downstream ambient flow will increase as A_D increases, and hence the strength of the upstream flow c will increase correspondingly. Putting this mathematically, supposing the variance of u_D to be small, we may approximate (3.34) by $F \approx A_D\overline{u_D}^2 - c^2$, where $\overline{u_D}$ is the mean downstream ambient velocity, and then

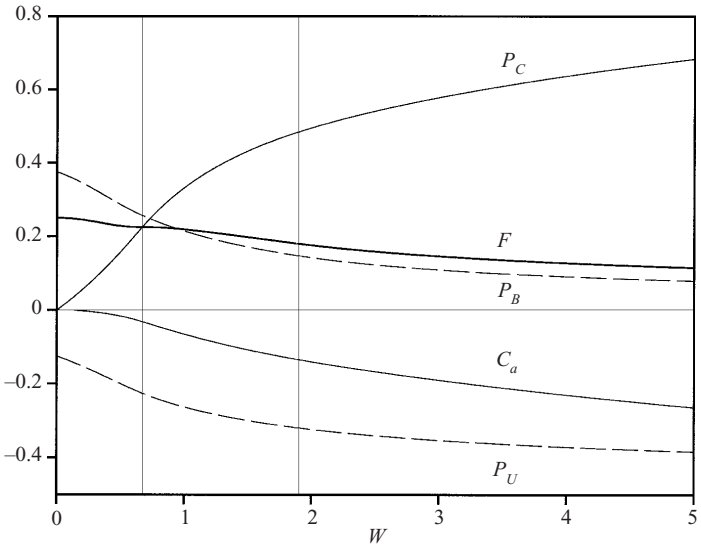

FIGURE 10. The variation of the various terms in the flow-force balance equation (3.34) with W.

using continuity of ambient fluid volume flux $\overline{u_D}A_D = c$ gives:

$$c^2 \approx FA_D(1 - A_D)^{-1}, \tag{3.36}$$

indicating that c will increase with increasing A_D provided that F, if decreasing, does not decrease at a rate faster than the rate of increase of the factor on the right-hand side of (3.36).

4. The one-layer solution

The results of the previous section show that when the ambient fluid has finite-depth, there is only one possible non-dissipative flow state for each value of W. Other flow states must either involve dissipation of energy or momentum, or violate some other assumption made in the theory. In the one-layer limit, however, non-dissipative solutions are also possible, essentially because the flow-force condition is degenerate in this case, in the sense that no information is provided by this equation to the accuracy of the one-layer approximation. This means the solution is fixed by the requirements of energy conservation alone. However, since there is one less constraint equation, one variable is left free, which here will be taken to be the value of the wall-depth h_0.

Let

$$\eta(y) = h(y)/H = O(\varepsilon), \tag{4.1}$$

with the limit $\varepsilon \to 0$ to be taken subsequently. Conservation of volume flux in the ambient fluid then indicates that

$$u_D(y) = c + O(\varepsilon), \tag{4.2}$$

and

$$\Delta Y(y) = O(\varepsilon). \tag{4.3}$$

To write the constraint equations in terms of $O(1)$ quantities, introduce the rescalings:

$$\eta(y) = \varepsilon\zeta(y), \quad c = \varepsilon^{1/2}c_0, \quad W = \varepsilon^{1/2}W_0, \tag{4.4}$$

where $\zeta(y) = h(y)/h_0$, $c_0 = c_f/(g'h_0)^{1/2}$ and $W_0 = B/R_0 = fB/(g'h_0)^{1/2}$ are considered to be $O(1)$. Then, using (4.2)–(4.4) with (2.41), it may be shown that at both the upstream and downstream locations, the flow force S is equal to within $O(\varepsilon)$. Physically, this indicates that the ambient fluid requires only an $O(\varepsilon)$ input of momentum in order to be accelerated around the gravity current. The flow-force balance is therefore satisfied to $O(\varepsilon)$, regardless of the form of the downstream flow structure. On the other hand, the Bernoulli equation (2.33) gives at $O(1)$

$$\tfrac{1}{2}c_0^2 = \begin{cases} \zeta(y) + W_0c_0y + O(\varepsilon), & y \in [0, b], \\ W_0c_0b + O(\varepsilon), & y \in [b, 1]. \end{cases} \tag{4.5a, b}$$

The left-hand side of this expression indicates that there is a uniform dynamic pressure drop downstream relative to the nose, by virtue of (4.2). This pressure drop must be balanced by the pressure on the interface, with (4.5a) indicating that this requires a linear interface profile. The same result could have been obtained by first noting from (4.2) and (2.12) that the downstream ambient fluid pressure is uniform to $O(\varepsilon)$; then by determining the value of this pressure using (2.28) applied in the ambient fluid along the right-hand wall from the stagnation point at the nose; and then by equating this value with that given by (2.14) applied on the interface. The second equation in (4.5) simply states that the pressure is continuous on the interface at $y = b$, and hence provides no further information.

Once the energy balance (4.5) has been written down, the one-layer solution follows directly. First, applying (4.5a) at $y = 0$ (where $\zeta = 1$) gives

$$c_0 = 2^{1/2}, \tag{4.6}$$

and then substituting this value back into (4.5a) gives

$$\zeta(y) = 1 - 2^{1/2}W_0y. \tag{4.7}$$

Note that the form of the solution in (4.6)–(4.7) is consistent with that given to leading order by the general solution for the interface and velocity profiles (2.22)–(2.23). From (4.7), the onset of Case B occurs at $W_0 = 2^{-1/2}$, and thereafter the width of the gravity current

$$b = 2^{-1/2}W_0^{-1}, \tag{4.8}$$

which corresponds to a dimensional width of $2^{-1/2}R_0$. Note that, by definition, Case C does not occur in the one-layer case.

The value of the wall-depth based Froude number given by (4.6) is the same as that determined by Benjamin for the non-rotating one-layer case. This is because, as asserted in § 2, the energy balance at the right-hand wall relative to the forward stagnation point is unmodified by rotation. The value of c_0 given in (4.6) is also very close to the values of 1.55 and 1.45 predicted by the shock-wave theories of Stern *et al.* (1982) and Kubokawa & Hanawa (1984). Both formulations suppose a constant value of PV within the gravity current and will be discussed in Part 2 in the context of the solutions given there.

5. Summary and conclusions

The perfect-fluid theory developed in this paper illustrates several aspects of the dynamics of energy-conserving gravity currents in rotating channels. First, and perhaps most fundamental, is the fact that in the two-layer case, Coriolis forces play a major part in providing the motive force that enables the gravity current to progress through the ambient fluid, and so, with a similar use of terminology, 'gravity currents' in rotating systems may also be described as 'Coriolis currents'. Secondly, it was shown that in the two-layer rotating case, the flow of ambient fluid around the gravity current places important restrictions on the structure and propagation speed of the current. Steady-state non-dissipative solutions are possible for all levels of rotation, as expressed by the non-dimensional channel width $W = B/R$, with the solution being unique for each value of W. As the value of W increases, the combined constraints of momentum, energy and PV conservation, which are the dynamic constraints consistent with the perfect fluid approximation, require that: the depth of the gravity current at a proposed geostrophic upstream control point increases, reaching the full depth of the channel at $W = 1.90$; the current separates from the left-hand wall when $W = 0.67$ and thereafter has decreasing width, the width of the region of interfacial slope being a constant fraction of R for $W \geqslant 1.90$; and the non-dimensional propagation speed $c = c_f/(g'H)^{1/2}$ increases, asymptoting to unity for $W \to \infty$.

Although the total gravitational buoyancy force acting on the current decreases with increasing W, primarily owing to the effect of the decrease in the cross-sectional area of the current offsetting the effect of the increase in depth, the total pressure force due to the rest-frame Coriolis force (i.e. the 'rotational buoyancy') increases strongly with W. This increase in downstream pressure force is in large part counteracted by the along-channel Coriolis forces acting within the control volume, produced by the movement of ambient fluid around the current, and also by the upstream dynamic pressure drop produced by the speed of the oncoming ambient flow. As a result, the total motive force exerted on the ambient fluid remains approximately constant, actually decreasing slowly with increasing W. However, since the cross-sectional area of the ambient fluid at the control-section increases with W, it becomes easier for this motive force to accelerate the ambient fluid through the control section, with the result that the propagation speed increases.

For the one-layer case, the propagation speed is given by the same Froude number condition as in the non-rotating case, with this being established by the same balance between the dynamic pressure drop produced by the speed of propagation and the gravitational pressure drop produced by the depth of the current. As in the two-layer case, the rotational buoyancy force exerted on the current causes the pressure to decrease within the gravity current away from the right-hand wall. Since the pressure is uniform in the ambient fluid beneath the gravity current, the shape of the interface is determined by the condition that the rotational-buoyancy induced pressure gradient must be balanced by the hydrostatic pressure gradient, which for the present case of $u_c = 0$ requires the interface profile to be linear.

While we believe that the dynamics illustrated by the calculation presented here are those fundamental to the factors controlling the speed of propagation and structure of gravity currents in rotating channels, it must be emphasized that the calculation pertains to a highly idealized situation, and can only be viewed as a 'first-order' picture of the flow in real physical situations. Additional effects among those likely to be important in given situations are: shear-generated interfacial turbulence and

entrainment of ambient fluid into the gravity current; propagating interfacial waves and the effects of eddies and meanders produced by baroclinic instability; effects of ambient fluid stratification; the modulation of the production and destruction of gravity current fronts by ambient turbulence; the effects of finite upstream ambient flow and shear in opposing and supporting the propagation of the gravity current and altering the mixing characteristics; and the effects of non-rectangular channel geometry.

Although many of these factors have been investigated for gravity currents in non-rotating systems (Simpson 1997), or for more general types of buoyancy-driven flow in rotating systems (Griffiths 1986), their effect on the dynamics of the type of ageostrophic gravity current fronts considered here remain mostly unstudied. Although it may be possible that the present theory could be extended to address these aspects, as, for example, was done by Benjamin (1968) to examine the effect of dissipation in the non-rotating case, such extensions lie beyond the scope of the present study. An important issue in the context of the non-dissipative theory, however, is the effect of non-zero front-relative flow. In particular, for the approximation of $u_c = 0$ made here, the PV distribution within the current q_c is specified by the solution, being given by $q_c = f/h(y)$. Unless conditions in the region supplying buoyant fluid to the gravity current are such as to produce exactly this PV distribution, which is unlikely, a major redistribution of PV must occur in some adjustment region, or during some initial adjustment phase at the inception of the flow. Physically, there seems to be no reason why such an adjustment would produce the exact q_c profile necessary to support the $u_c = 0$ state, and so we must expect for general upstream conditions that u_c will be non-zero. In Part 2, we will consider this case, and will determine solutions for the case of q_c constant. Finally, in Part 3, we will report lock-release experiments designed to assess the validity of the perfect-fluid theory, particularly with regard to the predictions of front-speed, upstream flow structure, and the assumptions made concerning the quasi-steadiness of the flow and the existence of the geostrophic control point. Through these experiments it will also be possible to consider questions that cannot be addressed using the perfect-fluid theory, such as to what the structure of the flow is away from the control point, and how a gravity current of this type develops from the release of a finite volume of buoyant fluid, which is the case of most geophysical interest.

We are grateful to Joanne Holford, Justin Moston and David Smeed for useful discussions, and to three anonymous referees for helpful comments.

Appendix A. Experimental support for the existence of Benjamin's non-dissipative solution

Most experimental studies of non-rotating gravity currents have used the 'lock-exchange' or 'lock-release' technique, in which two fluids of different densities contained in a long horizontal channel are initially separated by a vertical barrier. The barrier is withdrawn and the two fluids adjust under gravity to form counter-flowing buoyant and dense gravity currents.

Baines, Rottman & Simpson (1985) used this technique to study gravity currents of air propagating into water-filled channels. When the lock depth H_0 was greater than $0.7H$, the air cavities adjusted to a shape similar to that in Benjamin's energy-conserving free-boundary solution shortly after the removal of the lock gate. The asymptotic upstream fractional current depth h/H was in the range 0.5–0.56. The

values of c were in the range 0.46–0.50, and were constant in each experiment for approximately 8 lock-lengths of propagation. It was shown that these values of h and c are consistent with a modification to Benjamin's non-dissipative calculation allowing for surface-tension effects.

Gröbelbauer, Fanneløp & Britter (1993) carried out full-depth lock-release experiments with miscible gases over a wide range of density ratios. The shape of the buoyant currents was shown to be very close to Benjamin's energy-conserving free-boundary solution, although the dense currents were more blunt-nosed and showed greater turbulence and mixing. A generalization of Benjamin's calculation for arbitrary density ratios was found to give good predictions of c for both buoyant and dense currents, although broke down for dense currents at high density ratios, since the ambient fluid density (an important factor in Benjamin's theory) goes to zero in this limit.

Many authors have carried out full-depth lock-release experiments with miscible Boussinesq fluids, typically saline water propagating into fresh water. The upper boundary in such experiments is typically a free surface (zero stress) and the lower boundary a solid surface (no-slip). Such flows develop in an asymmetric manner, with the front of the dense current being shallower and more turbulent than the surface front. The propagation speeds of both fronts are typically constant for approximately 10 lock-lengths of propagation (Rottman & Simpson 1983). In experiments carried out in large flumes at Reynolds numbers $Re \equiv (g'H)^{1/2}H/\nu \gtrsim 10^3$, Keulegan (1957) found $c = 0.462$ and Barr (1967) $c = 0.465$ for dense fronts propagating along solid surfaces. Similar values have been reported elsewhere (Middleton 1966; Rottman & Simpson 1983; Hacker *et al.* 1996). Only Barr (1967) has reported values of c for free-surface currents, finding $c = 0.59$. The leading edge of the dense underflow in such experiments is typically characterized by a raised forward part called the 'head', behind which there is a shallower region of turbulence and mixing. Both regions can be unsteady and for this reason consistent measurements of depth are difficult. Only Keulegan (1957) has reported detailed measurements of current depth from lock-exchange experiments. He found that for higher values of Re, the fractional depth of the head of the underflowing current h/H decreased slowly from approximately 0.43 to 0.37 before decreasing more sharply as the current decelerated. The depth of the region to the rear of the head was approximately half that of the head. Similar values have been reported elsewhere in the literature, although in less detail (Middleton 1966; Simpson & Britter 1979; Rottman & Simpson 1983; Hacker *et al.* 1996).

Several authors, including Benjamin himself, have argued that fractional depths greater than 0.347 may not occur in practice, since Benjamin's (1968) dissipative calculation indicates the ambient flow to be supercritical in this range. However, depths close to half-height evidently occur in the non-Boussinesq flows discussed above, and the apex of the head in Boussinesq miscible gravity currents exceeds 0.347. In addition, values of c in both cases are very close to Benjamin's non-dissipative value.

Recently, Hartel, Meiburg & Necker (2000) have reported high-resolution direct numerical simulations of salt-into-fresh water lock-release gravity currents at $Re = O(10^4)$. These simulations used symmetric top and bottom boundary conditions, and the upper and lower gravity current fronts developed in a similar manner. For no-slip boundaries, both fronts had head heights close to $0.55H$ and steady propagation speeds $c = 0.46$ for the largest values of Re considered. For slip boundaries, the propagation speed tended to $c = 0.49$ for high Re. Strikingly, in two-dimensional simulations with slip boundaries, the shape of the free-streamline connecting to the forward stagnation point had shape nearly identical to Benjamin's energy-conserving

free-boundary solution, before becoming disrupted by interfacial waves near the apex of the head.

Appendix B. Expression for the downstream flow-force

Here we give a method to obtain the expression for the downstream flow-force (2.43). First, from (2.41) the downstream flow-force

$$S_D = \int_{b_0}^{1} (u_D^2 + p_D)(1-\eta)\,\mathrm{d}y + \int_0^b \mathrm{d}y \int_{1-\eta(y)}^{1} p_c\,\mathrm{d}z + W\int_{b_0}^{1} y u_D (1-\eta)\,\mathrm{d}y.$$

Integrating the second integral once by parts and using the volume-flux expression (2.37) and rearranging the pressure terms gives

$$S_D = \int_{b_0}^{1} (u_D^2(1-\eta) + p_D)\,\mathrm{d}y + \int_{b_0}^{b} \left(-p_D\eta + \int_{1-\eta(y)}^{1} p_c\,\mathrm{d}z\right)\mathrm{d}y + \int_0^{b_0} \mathrm{d}y \int_{1-\eta(y)}^{1} p_c\,\mathrm{d}z + Wc - \int_{b_0}^{1} \mathrm{B}_D\,\mathrm{d}y.$$

Substituting the solution for the downstream pressure (2.14) and (2.16) into the second integral, gives, for general $P(y)$,

$$S_D = Wc + \int_{b_0}^{1} (u_D^2(1-\eta) + p_D - \mathrm{B}_D)\,\mathrm{d}y + \int_{b_0}^{b} \tfrac{1}{2}\eta^2\,\mathrm{d}y - \tfrac{1}{2}b_0 - \int_0^{b_0} P\,\mathrm{d}y.$$

Next, expanding B_D according to (2.31) and rearranging terms, gives (notice the cancellation of the pressure terms in the first integral)

$$S_D = \tfrac{1}{2}Wc(1+b_0^2) - \tfrac{1}{2}b_0 + \tfrac{1}{2}U^2(1-b) + \int_{b_0}^{b} (\tfrac{1}{2}u_D^2 - \eta u_D^2 + \tfrac{1}{2}\eta^2)\,\mathrm{d}y - \int_0^{b_0} P\,\mathrm{d}y, \quad \text{(B 1)}$$

which shows that $P(y)$ only affects S_D through its integral over the interval $[0, b_0]$, with elsewhere the pressure terms cancelling exactly with terms arising from the Coriolis force term. Physically, this indicates that changes in the total along-channel Coriolis force due to accelerations produced by the rotational buoyancy-induced pressures acting downstream are exactly balanced by the corresponding changes in the total pressure force acting across the downstream cross-section.

For $u_c = 0$, the integrand of the second integral in (B 1) may be written as an exact differential using the geostrophic and PV equations (2.20)–(2.21), which together with the expression for $P(y)$, (2.18), gives, from (B 1),

$$S_D = \tfrac{1}{2}Wc - \tfrac{1}{2}b_0 + \tfrac{1}{2}U^2(1-b) + \tfrac{1}{2}W^{-1}[\tfrac{2}{3}u_D^3 - u_D\eta]_{b_0}^{b}.$$

This expression may be simplified further by noting from the Bernoulli equations, (2.35)–(2.36) that:

$$[\tfrac{2}{3}u_D^3 - u_D\eta]_{b_0} = \tfrac{1}{6}u_0^3,$$

$$[\tfrac{2}{3}u_D^3 - u_D\eta]_{b} = \tfrac{1}{6}U^3 + Wc\,U - W\,U^2(1-b),$$

and hence,

$$S_D = \tfrac{1}{2}c(U+W) - \tfrac{1}{2}b_0 + \tfrac{1}{2}W^{-1}[\tfrac{1}{3}u_D^3]_{b_0}^{b}, \quad \text{(B 2)}$$

which is (2.43).

REFERENCES

Alhnäs, K., Royer, T. C. & George, T. H. 1987 Multiple dipole eddies in the Alaskan Coastal Current detected with Landsat Thematic Mapper data. *J. Geophys. Res.* **92** (C12), 13 041–13 047.

Baines, W. D., Rottman, J. W. & Simpson, J. E. 1985 The motion of constant-volume air cavities in long horizontal tubes. *J. Fluid Mech.* **161**, 313–327.

Barr, D. I. H. 1967 Densimetric exchange flow in rectangular channels. III large scale experiments. *Houille Blanche* **6**, 619–631.

Batchelor, G. K. 1967 *An Introduction to Fluid Dynamics*. Cambridge University Press.

Benjamin, T. B. 1968 Gravity currents and related phenomena. *J. Fluid Mech.* **31**, 209–248.

Britter, R. E. & Simpson, J. E. 1978 Experiments on the dynamics of a gravity current head. *J. Fluid Mech.* **88**, 223–240.

Gill, A. E. 1982 The hydraulics of rotating-channel flow. *J. Fluid Mech.* **80**, 641–671.

Griffiths, R. W. 1986 Gravity currents in rotating systems. *Annu. Rev. Fluid Mech.* **18**, 59–89.

Griffiths, R. W. & Hopfinger, E. J. 1983 Gravity currents propagating along a lateral boundary in a rotating fluid. *J. Fluid Mech.* **134**, 357–399.

Gröbelbauer, H. P., Fanneløp, T. K. & Britter, R. E. 1993 The propagation of intrusion fronts of high density ratio. *J. Fluid Mech.* **250**, 669–687.

Hacker, J. N. 1996 Gravity currents in rotating channels. PhD thesis, University of Cambridge.

Hacker, J. N. 1998 Ageostrophic gravity current fronts in the oceans. Unpublished, available on request.

Hacker, J. N. & Linden, P. F. 2002*a* Gravity currents in rotating channels. Part 2. Effects of front-relative flow. In preparation.

Hacker, J. N. & Linden, P. F. 2002*b* Gravity currents in rotating channels. Part 3. Laboratory experiments. In preparation.

Hacker, J. N., Linden, P. F. & Dalziel, S. B. 1996 Mixing in lock-release gravity currents. *Dyn. Atmos. Oceans* **24**, 183–195.

Hartel, C., Meiburg, E. & Necker, F. 2000 Analysis and direct numerical simulation of the flow at a gravity current head. Part 1. Flow topology and front speed for slip and no-slip boundaries. *J. Fluid Mech.* **418**, 189–212.

Hickey, B. M., Thompson, R. E., Yih, H. & LeBlond, P. H. 1991 Velocity and temperature fluctuations in a buoyancy-driven current off Vancouver Island. *J. Geophys. Res.* **96** (C6), 10 507–10 538.

Ikeda, M., Johannessen, J. A., Lygre, K. & Sandven, S. 1989 A process study of mesoscale meanders and eddies in the Norwegian Coastal Current. *J. Phys. Oceanogr.* **19**, 20–35.

Keulegan, G. B. 1957 An experimental study of the motion of saline water from locks into fresh water channels. *Natl Bur. Stand. Rep.* 5168.

Kubokawa, A. & Hanawa, K. 1984 A theory of semigeostrophic gravity waves and its application to the intrusion of a density current along the coast of a rotating fluid. Part II: The propagation of a density current along the coast in a rotating fluid. *J. Oceangr. Soc. Japan* **40**, 260–270.

Lavín, M. F., Godínez, V. M. & Alvarez, L. G. 1998 Inverse-estuarine features of the Upper Gulf of California. *Estuarine, Coastal and Shelf Science* **46**, 769–795.

LeBlond, P. H., Ma, H., Doherty, F. & Pond, S. 1991 Deep and intermediate water replacement in the Strait of Georgia. *Atmosphere–Ocean* **29**, 288–312.

Middleton, G. V. 1966 Experiments on density and turbidity currents I. Motion of the head. *Can. J. Earth Sci.* **3**, 523–546.

Nof, D. 1987 Penetrating outflows and the dam-breaking problem. *J. Marine Res.* **45**, 557–577.

O'Donnell, J. 1993 Surface fronts in estuaries: A review. *Estuaries* **16**, 12–39.

Rottman, J. W. & Simpson, J. E. 1983 Gravity currents produced by instantaneous releases of a heavy fluid in a rectangular channel. *J. Fluid Mech.* **135**, 95–110.

Royer, T. C. 1981 Baroclinic transport in the Gulf of Alaska II. A fresh-water driven coastal current. *J. Mar. Res.* **39**, 251–266.

Saunders, P. M. 1994 The flux of overflow water through the Charlie–Gibbs Fracture Zone. *J. Geophys. Res.* **99** (C6), 12 343–12 355.

Schär, C. 1993 A generalisation of Bernoulli's theorem. *J. Atmos. Sci.* **50**, 1437–1443.

Signori, S. R., Münchow, A. & Haidvogel, D. 1997 Flow dynamics of a wide Arctic canyon. *J. Geophys. Res.* **102** (C8), 18 661–18 680.

Simpson, J. E. 1997 *Gravity Currents in the Environment and in the Laboratory*, 2nd edn. Cambridge University Press (1st edn. 1987, Ellis-Hornwood, Chichester).

Simpson, J. E. & Britter, R. E. 1979 The dynamics of the head of a gravity current advancing over a horizontal surface. *J. Fluid Mech.* **94**, 447–495.

Simpson, J. E. & Linden, P. F. 1989 Frontogenesis in a fluid with horizontal density gradients. *J. Fluid Mech.* **202**, 1–16.

Stern, M. E., Whitehead, J. A. & Hua, B. L. 1982 The intrusion of a density current along the coast of a rotating fluid. *J. Fluid Mech.* **123**, 237–265.

Takeoka, H., Akiyama, H. & Kikuchi, T. 1993 The Kyucho in the Bungo Channel, Japan. Periodic intrusions of oceanic warm water. *J. Ocean. Soc. Japan* **49**, 369–382.

Volkert, H., Weikman, L. & Tafferner, A. 1991 The Papal Front of 3 May 1987: A remarkable example of frontogenesis near the Alps. *Q. J. R. Met. Soc.* **117**, 125–150.

Wang, D.-P. 1985 Numerical study of gravity currents in a channel. *J. Phys. Oceanogr.* **15**, 299–305.